Highlights

Estimation of parameters for solar cells with S–shaped current–voltage characteristics using meta–heuristic algorithms

Oleg Olikh

- Proposed deep learning-based method to predict iron contamination in Si-SC by using IV curve.
- The simulated IV characteristics are used to create training and test datasets.
- The DNN's configurations are proposed.
- The mean squared relative error of prediction is up to 0.005.

Estimation of parameters for solar cells with S–shaped current–voltage characteristics using meta–heuristic algorithms

Oleg Olikh

Taras Shevchenko National University of Kyiv, 64/13, Volodymyrska Street, Kyiv, 01601, Ukraine

ARTICLE INFO

Keywords:
Ideality factor
Silicon
n^+–p–p^+ structure
SCAPS
Iron contamination
Ma

ABSTRACT

Defect-assisted recombination processes frequently limit the photovoltaic device performance. The low-cost and express methods of impurity contamination control are in demand at solar cell manufacturing. In this paper, we applied deep learning-based approach to extract the iron concentration in silicon solar cell from an ideality factor values.

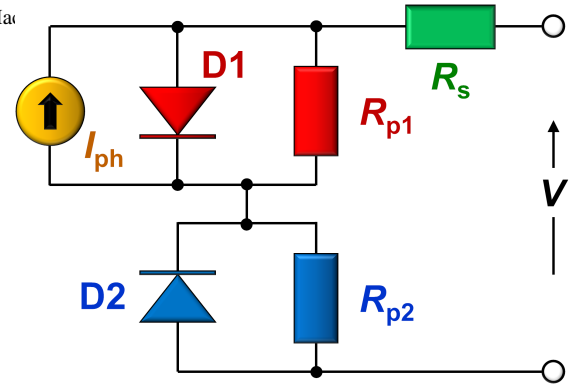

Figure 1: The opposed two–diode equivalent–circuit model of a solar cell.

1. Introduction

[1]

2. Problem definition

2.1. Solar cell model

Fig. 1 vividly reveals the structure of the used model [2]. It can be seen from the figure that model contains a current source accompanied by a diode D1, a shunt resistor R_{p1} to show the leakage current, and a series resistor R_s to consider the losses associated with the load current. Besides, the second diode D2 with a second parallel resistance R_{p2} is placed opposite to the first one and is essential to simulate the non-ideal effects of the active layer/cathode interface. In this model, D1 is responsible for the exponential behavior of the I–V curve, the main contribution of D2 is to simulate the S–shape. The analytical solution $V(I)$ of the opposed two–diode equivalent circuit model was obtained [3] using Lambert W-function [4]:

$$\begin{aligned} V = {} & (I+I_{ph}+I_{01})R_{p1} \\ & -\frac{n_1kT}{q}W\left\{\frac{qI_{01}R_{p1}}{n_1kT}\exp\left[\frac{qR_{p1}(I+I_{ph}+I_{01})}{n_1kT}\right]\right\} \\ & +\frac{n_2kT}{q}W\left\{\frac{qI_{02}R_{p2}}{n_2kT}\exp\left[-\frac{qR_{p2}(I-I_{02})}{n_2kT}\right]\right\} \\ & +(I-I_{02})R_{p2}+IR_s\,, \end{aligned} \tag{1}$$

where I_{01} and I_{02} are the saturation currents and n_1 and n_2 are the ideality factors for D1 and D2 respectively, and I_{ph} is the ideal photocurrent. Thus, the model employs eight lumped parameters (I_{01}, n_1, R_{p1}, I_{02}, n_2, R_{p2}, R_s, and I_{ph}) that need to be determined from the I-V curve. Thus, from an optimization perspective, the dimension of the problem is $D = 8$.

The expression (1) has a drawback in that it tends to stray from the range of numbers that can be accommodated by the standard 64-bit floating-point format owing to the presence of exponential functions for larger numbers. To overcome this drawback, the use of the g–function $g(x) = \ln(W(\exp(x)))$ was suggested [5]. The analytical solution $V(I)$ using the g–function is as follows [5]

$$\begin{aligned} V(I) = {} & IR_s+\frac{n_1kT}{q}g(x_1)-\frac{n_2kT}{q}g(x_2) \\ & -\frac{n_1kT}{q}\ln\left[\frac{qI_{01}R_{p1}}{n_1kT}\right]+\frac{n_2kT}{q}\ln\left[\frac{qI_{02}R_{p2}}{n_2kT}\right], \end{aligned} \tag{2}$$

with

$$x_1 = \ln\left(\frac{qI_{01}R_{p1}}{n_1kT}\right)+\frac{q(I+I_{ph}+I_{01})R_{p1}}{n_1kT}\,, \tag{3}$$

and

$$x_2 = \ln\left(\frac{qI_{02}R_{p2}}{n_2kT}\right)-\frac{q(I-I_{02})R_{p2}}{n_2kT}\,. \tag{4}$$

We used Eqs. (2)–(4) both for simulation IV curves and during the approximation procedure. The g–function was evaluated by using iterative procedure [5].

2.2. Synthetic IV curves

The research involved the parameter estimation of solar cells using meta-heuristic algorithms based on synthetic IV characteristics simulated using the opposed two–diode model. This approach allows for assessing the accuracy of the employed optimization methods, as the simulation was performed using known parameter values.

olegolikh@knu.ua (Oleg Olikh)
ORCID(s):

In first part of the study, a detailed analysis was conducted on a single IV curve, evaluating the performance of meta–heuristic algorithms for parameter estimation in a one–time application mainly. Additionally, the suitability of employing two different fitness functions was examined. In the second part, we simulated a set of IV characteristics and evaluated the average performance metrics of various algorithms.

2.2.1. *Single–IV case*

Previous studies have demonstrated [6, 7] that when the ideality factor of D2 is either equal to or significantly larger than n_1, ($n_1 = n_2 = 1.92$ or $n_1 = 1.00$, $n_2 = 3.00$) the nonlinear least–squares method successfully determines a set of equivalent circuit parameters that accurately replicate the experimental data of an organic photovoltaic cell. Therefore this approach does not allow for distinguishing between similar IV curves obtained from solar cells with different parameters. To overcome this issue, Tada [7] successfully employed Bayesian estimation of parameters. To assess the capabilities of meta-heuristic methods in overcoming additional similar challenges, they were applied to a IV curve corresponding to such a problematic case. The parameter values were taken from [7]:

$$\begin{aligned} I_{01} &= 1.6 \cdot 10^{-6}\,\text{mA}, \\ n_1 &= 1.92, \\ R_{\text{p1}} &= 190\,\Omega, \\ I_{02} &= 0.16\,\text{mA}, \\ n_2 &= 1.92, \\ R_{\text{p2}} &= 190\,\Omega, \\ R_{\text{s}} &= 45\,\Omega, \\ I_{\text{ph}} &= 8\,\text{mA}, \end{aligned} \tag{5}$$

and the IV curve was simulated over a range of 0-0.8 V with step 10 mV at $T = 300$ K. The simulation result is presented on Fig. 2 by symbols.

2.2.2. *IV–set case*

Employing various meta–heuristic algorithms to analyze a single IV curve is insufficient to obtain comprehensive insights into the methods' efficacy in parameter estimation. The accuracy of parameter determination is closely tied to their absolute values. For instance, an increase in the R_{p} value can pose challenges for accurately estimating resistance because the shunt will have a lesser impact on the overall shape of IV curve. In addition, the ratio between the parameter values also plays a crucial role.

To test the methods across different parameter values, we generated synthetic data in a temperature range from 260 K to 350 K. During the simulation process, we considered various temperature dependencies of the parameters. We based our approach on known physical mechanisms but focused on achieving the diversity of parameter ratio instead of attempting to replicate real–life photovoltaic converters precisely. Furthermore, an S–shaped IV curve is observed

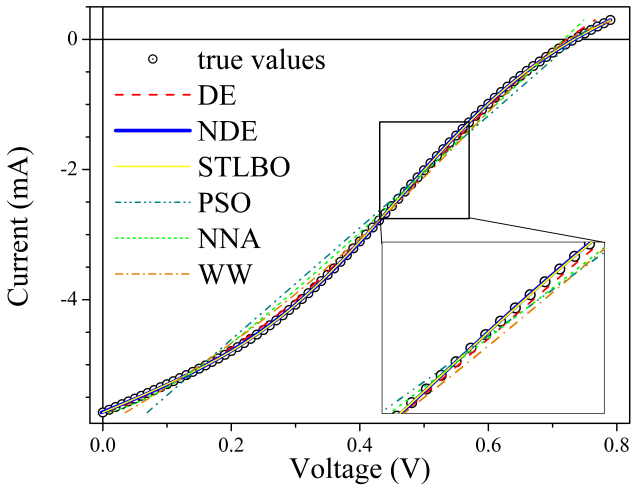

Figure 2: Fitting results (lines) for the simulated current-voltage characteristic (symbols). The values from Eq. (5) were assumed under simulation.

in solar cells of various types, and diverse charge transport mechanisms significantly complicate the selection of the only possible temperature dependence for each of the eight model parameters. Therefore, we assumed that the current conduction mechanism through D1 is close to tunneling, and hence, I_{01}, R_{p1}, and $n_1 kT$ remain constant, with $I_{01} = 0.015$ mA, $R_{\text{p1}} = 10^4\ \Omega$, $n_1 kT = 7$ eV. In the case of D2, the thermionic emission current was suggested and I_{02} and n_2 increased and decreased, respectively, with temperature rise [8]:

$$I_{02} = I_{002} \exp\left(-\frac{E_I}{kT}\right), \tag{6}$$

$$n_2 = 1 + \frac{T^*}{T}, \tag{7}$$

where I_{002}, E_I, and T^* are the constants which are independent of temperature. The values of $I_{002} = 500$ A, $E_I = 0.40$ eV, and $T^* = 500$ K were used. For R_{p2}, an exponential temperature dependence was employed, as it is widely observed [9] in modern solar cells for the shunt resistance:

$$R_{\text{p2}} = R_{\text{p20}} \exp\left(\frac{E_R}{kT}\right). \tag{8}$$

with $R_{\text{p20}} = 9$ mΩ, $E_R = 0.32$ eV. The linear temperature dependencies is expected for both I_{ph} [10, 11] and R_{s} [12, 13]:

$$y = y_0[1 + \text{TC}_y(T - 300)], \tag{9}$$

where $y = I_{\text{ph}}$ or R_{s}, y_0 is the parameter value at room temperature, TC_y is the temperature coefficient of parameter. For most types of monocrystalline silicon solar cells, the $\text{TC}_{I_{\text{ph}}}$ typically ranges from around $-0.0004\ \text{K}^{-1}$ [14]. However, as the base thickness decreases, the temperature coefficient can increase to $-0.0014\ \text{K}^{-1}$ [15]. For hydrogenated amorphous

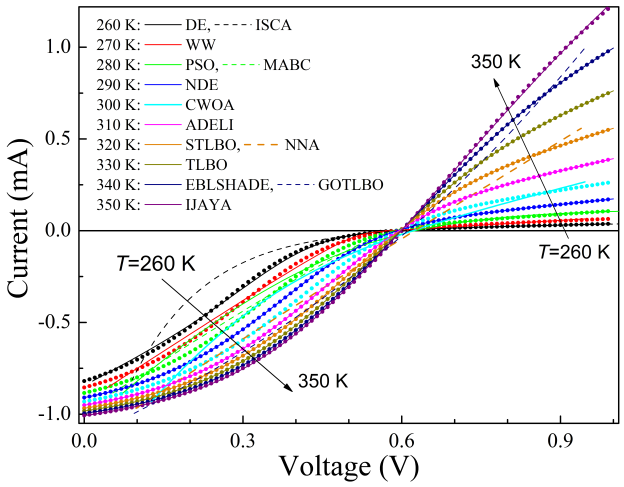

Figure 3: Fitting results (lines) for the simulated current-voltage characteristic (symbols). The values from Sec. 2.2.2 were assumed under simulation.

silicon solar cells, $\mathrm{TC}_{I_{\mathrm{ph}}}$ is equal to -10^{-3} K^{-1} [16]. For organic solar cells, the temperature coefficient can reach a magnitude of -0.003 K^{-1} [17]. During the simulation, we assumed $\mathrm{TC}_{I_{\mathrm{ph}}} = -10^{-3}$ K^{-1}. Furthermore, the values of $I_{\mathrm{ph0}} = 1$ mA, $\mathrm{TC}_{R_{\mathrm{s}}} = 0.02$ K^{-1}, and $R_{\mathrm{s0}} = 50\ \Omega$ were used.

The set of I–V data was composed of 10 curves, which were simulated at 10 K intervals from 260 to 350 K; in this case, n_1, I_{02}, n_2, R_{p2}, R_{s}, and I_{ph} varied from 6.37 to 4.73, from 9 to 880 μA, from 2.92 to 2.43, from $1.4 \cdot 10^4$ to 360 Ω, from 10 to 100 Ω, and from 0.96 to 1.05 mA, respectively. The simulation results are presented on Fig. 3 by symbols.

2.3. Meta-heuristic algorithms

In the literature, meta-heuristics are frequently categorized based on their sources of inspiration. This categorization involves incorporating elements of true simulations and principles that incorporate stochasticity, with the objective of emulating diverse characteristics observed in biological behavior, the lives of creatures in nature, human behavior, or natural phenomena. On this basis, any meta-heuristic algorithm can fall into one of the following main classes [18, 19, 20]: evolution-based methods (emulate the principles of evolutionary behavior observed in creatures in nature by relying on the concept of survival of the fittest), swarm intelligence–based methods (simulate the collective, dynamic, intelligent, and concerted gregarious conduct of collections of flocks or communities found in nature), bio–based methods (use biological processes unrelated to group behavior), chemical & physical–based methods (originate from the physical phenomena or chemical laws that exist in the universe), human-society–based methods (inspired by human beings, including various activities such as thinking and social behavior), and math–based methods (borrow the mathematical functions). Generally, there are hundreds of meta-heuristic optimization methods available. While we acknowledge that our selection may not be fully comprehensive, we utilized 14 methods, representing all classes mentioned above, to tackle the parameter estimation task within the framework of the opposed two-diode model for a solar cell. Hereafter, we provide a succinct description of each method alongside the parameters employed during the fitting process.

Differential evolution (**DE**). DE is one of the classical methods, and it is based on the natural selection law and uses the randomly generated initial population, differential mutation, and probability crossover [21]. During the implementation, we employed a penalty function suggested by Ishaque *et al* [22]. Besides, according to Wang and Ye [21], the values of mutation scaling factor $F = 0.8$, crossover rate $Cr = 0.3$, and population size $Np = 8 \times D = 64$ were used in this work.

Adaptive differential evolution with the Lagrange interpolation argument (**ADELI**). The method is based on DE, which integrates an adaptive local search scheme with Lagrange interpolation [23]. This incorporation aims to enhance the exploitation capability and accelerate the convergence speed. In ADELI, the scaling factor and crossover rate are set to self–adapting to optimize the results. We used parameter values recommended by Huang *et al* [23] during the implementation process. Additionally, we set Np to 64 for our numerical experiments.

Differential evolution with neighborhood–based adaptive evolution mechanism (**NDE**). The method uses a mutation strategy, which takes into account neighborhood and individual information, and an adaptive evolution mechanism [24]. The determination of F and Cr values is achieved through the utilization of the weighted adaptive procedure [25], and an adaptive adjustment of the population size is implemented using a simple reduction method (from $10 \times D = 80$ to 5).

Success history based DE with hybridization mutation strategies and population size reduction (**EBLSHADE**). The method is the hybridization framework between *pbest* and *ord_pbest* mutation strategies and stores a set of Cr and F values that have performed well in the recent past [26]. A linear Np reduction (from $18 \times D = 144$ to 4) is used as well.

Particle swarm optimization (**PSO**). It is another classic method based on observations of the social behavior of animals, such as bird flocking, fish schooling, and swarm theory. According to Ye et al. [27], the values of learning factors $l_1 = l_2 = 2$, the final weight and the initial weight $w_{max} = 0.9$, $w_{min} = 0.4$, and $Np = 15 \times D = 120$ are used in this work.

The *modified artificial bee colony* (**MABC**) algorithm is based on the intelligent foraging behavior of honey bee swarms [28]. The control parameters include the population size ($Np = 8 \times D = 64$) and the maximum number of generations after which each non-improved food source is to be discarded ($L_{imit} = 36$).

Chaotic Whale Optimization Algorithm (**CWOA**). WOA draws inspiration from the hunting behavior of humpback whales [29]. On the other hand, CWOA employs chaotic

maps to compute and dynamically adjust its internal parameters [30]. In our study, we utilized the Singer chaotic map and set $Np = 100$ for the identification of the parameters of the solar cell.

The *Neural Network Algorithm* (**NNA**) is a meta-heuristic algorithm that draws inspiration from both biological nervous systems and artificial neural networks [31]. The recommended [31] value $Np = 50$ is used in our paper.

The *teaching learning based optimization* (**TLBO**) algorithm employs the concept of passing on knowledge within a classroom. Similar to learners acquiring knowledge from a teacher and interacting with their peers, TLBO incorporates such interactions [32]. In this study, a value of $Np = 100$ is utilized.

Generalized oppositional teaching learning based optimization (**GOTLBO**). This method integrates a concept that incorporates both the current estimate and its opposite estimate simultaneously into the original TLBO algorithm through the initialization step and generation jumping [33]. The values of jumping rate $Jr = 1.0$ and $Np = 20$ were used.

Simplified teaching-learning based optimization algorithm (**STLBO**). In STLBO, an elite strategy is employed to improve the searching capability, and a the chaotic map is used to enrich the uniformity of random values in the mutation phase [34]. The logistic chaotic map and $Np = 20$ were used.

Water wave optimization (**WWO**) takes inspiration from shallow water wave models and borrows ideas from wave propagation, refraction, and breaking [35]. WWO is easy to implement with a small-size population, and there are four control parameters: the maximum wave height h_{max}, the wavelength reduction coefficient α, the breaking coefficient β, and the maximum number k_{max} of breaking directions. According to Zheng [35], we used the values $h_{max} = 6$, $\alpha = 1.026$, $Np = 10$, $k_{max} = \min(12, D/2) = 4$, and β linearly decreased from 0.25 to 0.001.

Improved JAYA (**IJAYA**). Jaya algorithm is based on the concept that the solution obtained for a given problem should move toward the best solution and should avoid the worst solution and does not require any algorithm-specific parameter [36]. In IJAYA, a self-adaptive weight is introduced to adjust the tendency of approaching the best solution and avoiding the worst solution; an experience-based learning strategy is employed to maintain the population diversity and enhance the exploration ability, and a chaotic elite learning method is proposed to refine the quality of the best solution in each generation [37]. The logistic chaotic map and $Np = 4 \times D = 32$ were used.

Improved sine cosine algorithm (**ISCA**). SCA based on simulating the behaviors of sine and cosine mathematical functions [38]. ISCA implementation included a modified position-updating equation based on inertia weight ($w_{start} = 1$, $w_{end} = 1$), a nonlinear conversion parameter strategy based on the Gaussian function ($a_{start} = 2$, $a_{end} = 0$) [39], the creation of the opposite population to jump out from the local optima with $Jr = 0.1$ [40], a greedy selection, and $Np = 30$.

The majority of the utilized algorithms demonstrate excellent performance when it comes to parameter estimation of solar cells within conventional models (single or double diode) [30, 21, 33, 37, 28, 27, 34, 32, 41, 42].

In meta-heuristic optimization methods, the quality of the extracted parameters is evaluated using the fitness function at every iteration. In our investigation, absolute error and square error fitness functions were under consideration:

$$F_{\mathrm{AE}}(Y) = \sum_{k=1}^{p} \left| V^{\mathrm{tr}}(I_k) - V^{\mathrm{cal}}(I_k, Y) \right| , \tag{10}$$

$$F_{\mathrm{SE}}(Y) = \sum_{k=1}^{p} \left[V^{\mathrm{tr}}(I_k) - V^{\mathrm{cal}}(I_k, Y) \right]^2 , \tag{11}$$

where $V^{\mathrm{tr}}(I_k)$ is the simulated value of voltage at current I_k, $V^{\mathrm{cal}}(I_k, Y)$ is the calculated values of voltage, which can be obtained by Eqs. (2)–(4), for given set of parameters (i.e. $Y = \{I_{01}, n_1, R_{\mathrm{p1}}, I_{02}, n_2, R_{\mathrm{p2}}, R_{\mathrm{s}}, I_{\mathrm{ph}}\}$) at current I_k, and p is the total number of voltage steps in the IV characteristic.

We executed each tested algorithm for $N_{\mathrm{runs}} = 51$ independent runs on each simulated IV curve to generate the statistical results. The search ranges were set as follows: $I_{01}(\mathrm{mA}) \in [10^{-13}, 1]$, $n_1 \in [0.5, 50]$, $R_{\mathrm{p1}}(\Omega) \in [10, 10^6]$, $I_{02}(\mathrm{mA}) \in [10^{-7}, 10]$, $n_2 \in [0.5, 50]$, $R_{\mathrm{p2}}(\Omega) \in [10, 5{\cdot}10^4]$, $R_{\mathrm{s}}(\Omega) \in [0.1, 1000]$, $I_{\mathrm{ph}}(\mathrm{mA}) \in [10^{-3}, 100]$.

2.4. Evaluation metrics

To better show the performance differences between compared algorithms, several evaluation metrics are considered, which can be described as follows:

1. Mean value (MEAN), median value (MEDIAN), standard deviance (STD), and interquartile range (IQR) for each two–diode model parameter y (y is one of $\{I_{01}, n_1, R_{\mathrm{p1}}, I_{02}, n_2, R_{\mathrm{p2}}, R_{\mathrm{s}}, I_{\mathrm{ph}}\}$). MEAN and MEDIAN are often used to measure the solution quality. The closer the obtained MEAN and MEDIAN values are to the actual parameter values, the closer the obtained solution is to the optimal solution. To quantify, we used the absolute percentage of error (APE):

$$\mathrm{APE}\,(y) = \left| \frac{y - y^{\mathrm{tr}}}{y^{\mathrm{tr}}} \right| , \tag{12}$$

   where y^{tr} is the parameter value used during the IV curve simulation. APE was calculated for y_i, obtained by one–run algorithm application (APE_i), MEAN ($\mathrm{APE}_{\mathrm{MEAN}}$), and MEDIAN ($\mathrm{APE}_{\mathrm{MEDIAN}}$). Reducing STD and IQR result in a more stable algorithm performance.
2. Another evaluation criterion used to compare the algorithms' performance is to compare their execution time. We used average run time t_{run} in seconds for an individual optimizer on one IV curve.

3. Root mean square percentage of error (RMSPE) is a statistical measure that indicates how well the fitted curve matches the actual IV curve:

$$\mathrm{RMSPE} = \sqrt{\frac{1}{p}\sum_{k=1}^{p}\left[\frac{V^{\mathrm{tr}}(I_k) - V^{\mathrm{cal}}(I_k, Y)}{V^{\mathrm{tr}}(I_k)}\right]^2}. \quad (13)$$

4. Wilcoxon signed-rank test is a nonparametric statistical test used for pairwise comparisons of algorithms. This test assigns a rank to all the scores considered as one group and then sums the ranks of each group.
5. Friedman, Friedman Aligned Ranks, and Quade tests are used for comparing the performance differences among optimization algorithms (multiple comparisons $1 \times N$ with a control method). Therefore, the average rankings of the algorithms according to the tests are reported. Besides, the post–hoc Finner, Holm, Hochberg, and Holland procedures are used to establish proper comparisons between each algorithm and a set of other algorithms.
6. Multiple Comparison Test (Friedman) with Shaffer's static, Nemenyi, and Holm procedures are employed to compute all possible pairwise comparisons between groups ($N \times N$) and identify the differences.

In the single–IV case, all nonparametric statistical tests were used to compare the performance of meta–heuristic algorithms in assessing each of the eight model parameters. The APE_i values were used, and the number of case problems in the study n was equal to $N_{\mathrm{runs}} = 51$. Additionally, algorithms were compared in terms of curve-fitting accuracy by using RMSPE values. Furthermore, tests were employed on a composite parameter. This parameter, referred to as "Comp" hereafter, includes $\mathrm{APE}_{\mathrm{MEDIAN}}$ for each of the eight defined model parameters, the median value for RMSPE, and t_{run}. This parameter may provide the most valuable insights for comparing algorithms. However, it is important to note that the value of n is only 10. According to Derrac *et al* [43], the number of case problems should be $n \geq 2k$, where k is the number of algorithms ($k = 14$ in our study). Therefore, the use of the Comp parameter is not strictly rigorous.

In the IV–set case, a comprehensive nonparametric statistical analysis of algorithms efficiency was performed on all parameters collected from all simulated curves. In this scenario, n had a value of 81:

$$n = 10\,T\mathrm{values} \times (8\,\mathrm{APE}_{\mathrm{MEDIAN}} + 1\,\mathrm{RMSPE}_{\mathrm{MEDIAN}}) + 1\,t_{\mathrm{run}}.$$

3. Numerical results and discussion

3.1. Comparison of algorithms time

In meta–heuristic algorithms, a different termination can be defined. For instance, a termination condition can be a specific number of iterations N_{it}, constraints on the number of fitness function evaluations N_{FE}, a specific rate of precision, a specific time, no sign of change in solutions after a specific number of iterations, or a combination of these cases [44]. In this study, the primary focus was on the accuracy of parameter estimation. Therefore to ensure that both exploration and exploitation processes could be fully realized by each algorithm with an equal opportunity, the termination criterion used was the absence of changes in the solution. Based on this condition, the required number of iterations N_{it} was determined, and the corresponding calculation time was measured t_{run}. In addition, the N_{FE} was evaluated.

Table 1
Comparison of optimization algorithms for single IV curve parameter estimation

Algorithm	N_{it}	N_{FE}	t_{run} (s)
DE	8000	1024000	42 ± 1
EBLSHADE	3000	444600	22 ± 1
ADELI	12000	1800000	93 ± 2
NDE	5000	430000	20.2 ± 0.3
MABC	8000	1024000	48 ± 11
TLBO	5000	1000000	56.1 ± 0.3
GOTLBO	6000	360000	15 ± 1
STLBO	13000	273000	13.8 ± 0.3
PSO	4000	480000	19 ± 3
IJAYA	30000	960000	37 ± 1
ISCA	5000	150000	6.5 ± 0.1
NNA	5000	250000	10.6 ± 0.5
CWOA	3000	300000	16.6 ± 0.5
WW	3000	35000	1.4 ± 0.1

All the applied algorithms have been coded and implemented in Embarcadero®Delphi 10.3 programming software. t_{run} was estimated by using WinAPI-functions *QueryPerformanceCounter()* and *QueryPerformanceFrequency()*. The experiments were performed on Windows 10 Pro 64-bit, 2.9 GHz AMD Ryzen 7 4800H CPU, and 8 GB RAM.

The obtained results are listed in Table 1. As can be seen from the table, the number of iterations required for an algorithm does not always correlate directly with the number of fitness function evaluations or computation time needed to converge. The reason is the unique features of each algorithm. The run time of the algorithms varies considerably, with a range of 1.5 seconds to 93 seconds. Notably, WW, ISCA, NNA, and STLBO converge the fastest, while ADELI, TLBO, and MABC require the most time.

3.2. Fitness function selection

To choose the more suitable fitness function, we evaluated each algorithm using the IV curve generated from the parameters provided in Eq. (5) with both F_{AE} and F_{SE} functions (see Eqs. (10) and (11)). Afterward, the results obtained using each of the functions were compared through pairwise comparisons. Table 2 gives the statistical results produced by Wilcoxon sign-rank test with a significant level $\alpha = 0.05$. A cell marked with the symbol "SE" indicates that evaluation of parameter specified in the column by the algorithm with F_{SE} outperforms result obtained by this algorithm with F_{AE}. A cell marked with the symbol "AE" indicates better results for function F_{AE}. In the case of the symbol "=", there is

Table 2
Wilcoxon signed ranks test results of fitness functions comparison with a level of significance $\alpha = 0.05$

Algorithm	Parameter								
	I_{01}	n_1	R_{p1}	I_{02}	n_2	R_{p2}	R_s	I_{ph}	RMSPE
DE	SE	SE	=	=	SE	SE	=	=	=
EBLSHADE	SE	=	=	=	=	=	=	=	AE
ADELI	SE	=	=	=	=	=	=	=	AE
NDE	=	=	=	=	=	=	=	SE	SE
MABC	=	SE	=	=	=	=	=	=	SE
TLBO	SE	SE	SE	SE	SE	SE	SE	SE	SE
GOTLBO	=	=	=	=	=	SE	=	=	=
STLBO	SE	=	=	=	=	=	=	=	AE
PSO	=	=	=	=	=	=	AE	=	=
IJAYA	AE	AE	=	=	SE	=	=	=	=
ISCA	=	=	=	=	=	=	=	=	=
NNA	=	=	=	=	=	=	=	=	SE
CWOA	=	=	SE	=	AE	=	=	=	SE
WW	=	=	SE	=	AE	=	=	=	SE

no significant difference between function F_{SE} and function F_{AE} aplication.

As evidenced in the provided data, utilizing the square error fitness function more frequently yields better outcomes in comparison to F_{AE}. In rare cases, the absolute error fitness function can enhance the alignment between the fitted and actual curves, as well as improve the accuracy of some parameter evaluations by PSO, IJAVA, CWOA, and WW algorithms. However, RMSPE is not the most crucial factor in determining model parameters, and the mentioned methods, as will be shown later, do not provide the highest accuracy. As such, the results presented in the following sections are exclusive to the application of the F_{SE} function. Therefore, it can be recommended that researchers consider the square error fitness function as a more effective and reliable option for the task of opposed two–diode model parameter evaluation.

3.3. Performance comparison

3.3.1. Evaluation of single–IV

3.3.2. Evaluation of IV–set

References

[1] D. Wolpert, W. Macready, No free lunch theorems for optimization, IEEE Trans. Evol. Comput. 1 (1997) 67–82.

[2] F. A. de Castro, J. Heier, F. A. Nüesch, R. Hany, Origin of the kink in current-density versus voltage curves and efficiency enhancement of polymer–C_{60} heterojunction solar cells, IEEE J. Sel. Top. Quantum Electron. 16 (2010) 1690–1699.

[3] B. Romero, G. del Pozo, B. Arredondo, Exact analytical solution of a two diode circuit model for organic solar cells showing S–shape using Lambert W–functions, Sol. Energy 86 (2012) 3026–3029.

[4] L. Lóczi, Guaranteed- and high-precision evaluation of the Lambert W function, Appl. Math. Comput. 433 (2022) 127406.

[5] K. Roberts, S. R. Valluri, On calculating the current-voltage characteristic of multi-diode models for organic solar cells, 2015.

[6] K. Tada, Parameter extraction from S-shaped current–voltage characteristics in organic photocell with opposed two-diode model: Effects of ideality factors and series resistance, Phys. Status Solidi A 212 (2015) 1731–1734.

[7] K. Tada, Bayesian estimation of equivalent circuit parameters of photovoltaic cell with S–shaped current–voltage characteristic, Phys. Status Solidi A 218 (2021) 2100403.

[8] S. M. Sze, M. Lee, Semiconductor Devices: Physics and Technology, John Wiley & Sons, Inc, New York, third edition, 2012.

[9] S. Kondratenko, V. Lysenko, Y. V. Gomeniuk, O. Kondratenko, Y. Kozyrev, O. Selyshchev, V. Dzhagan, D. R. T. Zahn, Charge carrier transport, trapping, and recombination in pedot:pss/n-si solar cells, ACS Appl. Energy Mater. 2 (2019) 5983–5991.

[10] M. A. Green, General temperature dependence of solar cell performance and implications for device modelling, Progress in Photovoltaics: Research and Applications 11 (2003) 333–340.

[11] R. Eberle, A. Fell, F. Schindler, J. Shahid, M. C. Schubert, Breakdown of temperature sensitivity of silicon solar cells by simulation input parameters, Sol. Energ. Mat. Sol. 219 (2021) 110836.

[12] H. Ibrahim, N. Anani, Variations of PV module parameters with irradiance and temperature, Energy Procedia 134 (2017) 276–285.

[13] F. Bradaschia, M. C. Cavalcanti, A. J. do Nascimento, E. A. da Silva, G. M. de Souza Azevedo, Parameter identification for PV modules based on an environment-dependent double-diode model, IEEE J. Photovolt. 9 (2019) 1388–1397.

[14] A. H. Tuan Le, R. Basnet, D. Yan, W. Chen, N. Nandakumar, S. Duttagupta, J. P. Seif, Z. Hameiri, Temperature-dependent performance of silicon solar cells with polysilicon passivating contacts, Sol. Energ. Mat. Sol. 225 (2021) 111020.

[15] O. Dupré, R. Vaillon, M. A. Green, Experimental assessment of temperature coefficient theories for silicon solar cells, IEEE J. Photovolt. 6 (2016) 56–60.

[16] Y. Riesen, M. Stuckelberger, F.-J. Haug, C. Ballif, N. Wyrsch, Temperature dependence of hydrogenated amorphous silicon solar cell performances, J. Appl. Phys. 119 (2016) 044505.

[17] A. Rana, A. Kumar, S. Chand, R. K. Singh, Exploring deep defect state impact on open circuit voltage of conventional and inverted organic solar cells, J. Appl. Phys. 124 (2018) 103101.

[18] M. Braik, A. Hammouri, J. Atwan, M. A. Al-Betar, M. A. Awadallah, White shark optimizer: A novel bio-inspired meta-heuristic algorithm for global optimization problems, Knowledge-Based Systems 243 (2022) 108457.

[19] J.-S. Pan, L.-G. Zhang, R.-B. Wang, V. Snášel, S.-C. Chu, Gannet optimization algorithm : A new metaheuristic algorithm for solving engineering optimization problems, Math. Comput. Simulation 202 (2022) 343–373.

[20] S. Zhao, T. Zhang, S. Ma, M. Chen, Dandelion optimizer: A nature-inspired metaheuristic algorithm for engineering applications, Eng. Appl. Artif. Intell. 114 (2022) 105075.

[21] K. Wang, M. Ye, Parameter determination of Schottky–barrier diode model using differential evolution, Solid-State Electron. 53 (2009) 234–240.

[22] K. Ishaque, Z. Salam, H. Taheri, A. Shamsudin, A critical evaluation of ea computational methods for photovoltaic cell parameter extraction based on two diode model, Solar Energy 85 (2011) 1768–1779.

[23] Q. Huang, K. Zhang, J. Song, Y. Zhang, J. Shi, Adaptive differential evolution with a lagrange interpolation argument algorithm, Inform. Sci. 472 (2019) 180–202.

[24] M. Tian, X. Gao, Differential evolution with neighborhood-based adaptive evolution mechanism for numerical optimization, Inform. Sci. 478 (2019) 422–448.

[25] R. Tanabe, A. S. Fukunaga, Improving the search performance of shade using linear population size reduction, in: 2014 IEEE Congress on Evolutionary Computation (CEC), pp. 1658–1665.

[26] A. W. Mohamed, A. A. Hadi, K. M. Jambi, Novel mutation strategy for enhancing SHADE and LSHADE algorithms for global numerical optimization, Swarm Evol. Comput. 50 (2019) 100455.

[27] M. Ye, X. Wang, Y. Xu, Parameter extraction of solar cells using particle swarm optimization, J. Appl. Phys. 105 (2009) 094502.

[28] N. Karaboga, S. Kockanat, H. Dogan, The parameter extraction of the thermally annealed schottky barrier diode using the modified artificial bee colony, Appl. Intell. 38 (2013) 279–288.

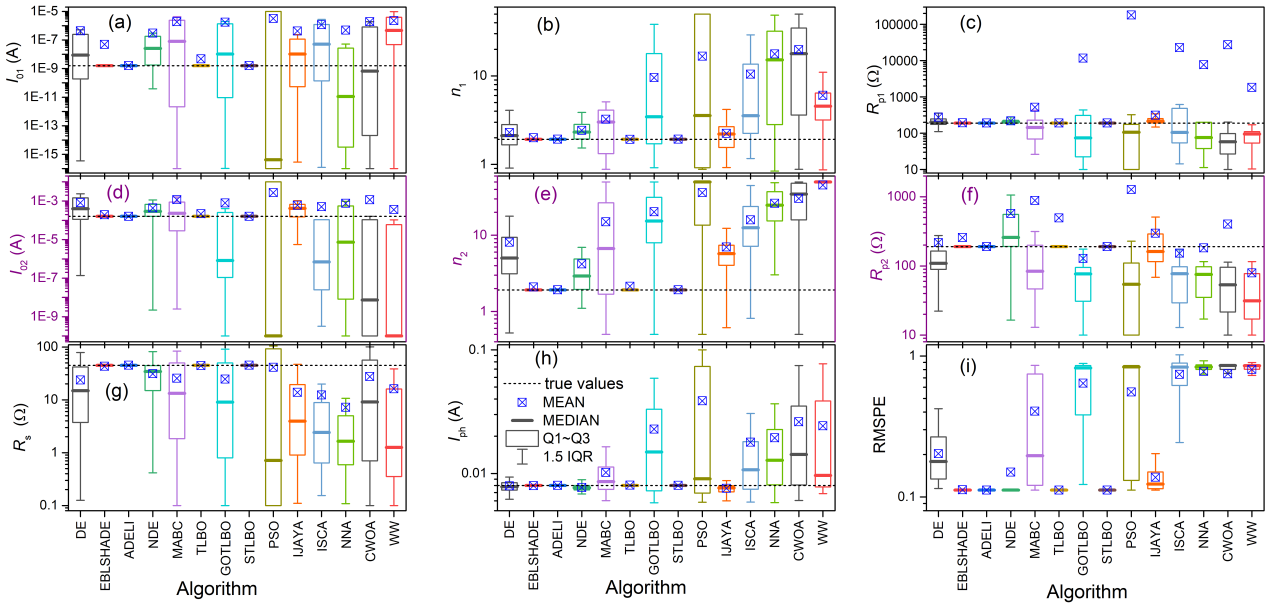

Figure 4: Box–plot of two–diode model parameter evaluation from single IV curve using different optimizers. Squares are the mean values, and dashed lines correspond to the true parameter values.

[29] S. Mirjalili, A. Lewis, The whale optimization algorithm, Adv. Eng. Software 95 (2016) 51–67.

[30] D. Oliva, M. Abd El Aziz, A. Ella Hassanien, Parameter estimation of photovoltaic cells using an improved chaotic whale optimization algorithm, Appl. Energy 200 (2017) 141–154.

[31] A. Sadollah, H. Sayyaadi, A. Yadav, A dynamic metaheuristic optimization model inspired by biological nervous systems: Neural network algorithm, Appl. Soft Comput. 71 (2018) 747–782.

[32] S. J. Patel, A. K. Panchal, V. Kheraj, Extraction of solar cell parameters from a single current–voltage characteristic using teaching learning based optimization algorithm, Applied Energy 119 (2014) 384–393.

[33] X. Chen, K. Yu, W. Du, W. Zhao, G. Liu, Parameters identification of solar cell models using generalized oppositional teaching learning based optimization, Energy 99 (2016) 170–180.

[34] Q. Niu, H. Zhang, K. Li, An improved TLBO with elite strategy for parameters identification of PEM fuel cell and solar cell models, Int. J. Hydrogen Energy 39 (2014) 3837–3854.

[35] Y.-J. Zheng, Water wave optimization: A new nature-inspired metaheuristic, Comput. Oper. Res. 55 (2015) 1–11.

[36] R. Rao, Jaya: A simple and new optimization algorithm for solving constrained and unconstrained optimization problems, International Journal of Industrial Engineering Computations 7 (2016) 19–34.

[37] K. Yu, J. Liang, B. Qu, X. Chen, H. Wang, Parameters identification of photovoltaic models using an improved JAYA optimization algorithm, Energy Conversion and Management 150 (2017) 742–753.

[38] S. Mirjalili, SCA: A sine cosine algorithm for solving optimization problems, Knowledge-Based Systems 96 (2016) 120–133.

[39] W. Long, T. Wu, X. Liang, S. Xu, Solving high-dimensional global optimization problems using an improved sine cosine algorithm, Expert Syst. Appl. 123 (2019) 108–126.

[40] S. Gupta, K. Deep, A hybrid self-adaptive sine cosine algorithm with opposition based learning, Expert Syst. Appl. 119 (2019) 210–230.

[41] P. P. Biswas, P. Suganthan, G. Wu, G. A. Amaratunga, Parameter estimation of solar cells using datasheet information with the application of an adaptive differential evolution algorithm, Renew. Energ. 132 (2019) 425–438.

[42] G. Xiong, J. Zhang, D. Shi, Y. He, Parameter extraction of solar photovoltaic models using an improved whale optimization algorithm, Energy Convers. Manage. 174 (2018) 388–405.

[43] J. Derrac, S. García, D. Molina, F. Herrera, A practical tutorial on the use of nonparametric statistical tests as a methodology for comparing evolutionary and swarm intelligence algorithms, Swarm Evol. Comput. 1 (2011) 3–18.

[44] V. Sahargahi, V. Majidnezhad, S. T. Afshord, Y. Jafari, An intelligent chaotic clonal optimizer, Appl. Soft Comput. 115 (2022) 108126.

Table 3
Adjusted p-values for Friedman, Friedman Aligned, and Quade tests in single–IV case. ADELI is the control algorithm, and the task of R_{p1} evaluation is under consideration.

Algorithm	Test	post-hoc procedure			
		Finner	Holm	Hochberg	Holland
GOTLBO	Friedman	<1E-13	<1E-13	<1E-13	<1E-13
	Friedman Aligned	2.23361E-09	6.87266E-09	6.87266E-09	6.87266E-09
	Quade	2.57827E-03	4.09880E-03	3.90245E-03	4.09117E-03
PSO	Friedman	<1E-13	<1E-13	<1E-13	<1E-13
	Friedman Aligned	<1E-13	<1E-13	<1E-13	<1E-13
	Quade	2.57827E-03	2.58134E-03	2.58134E-03	2.57827E-03
MABC	Friedman	6.35048E-13	1.61204E-12	1.61204E-12	1.61204E-12
	Friedman Aligned	7.88131E-06	2.97065E-05	2.97065E-05	2.97062E-05
	Quade	1.73550E-02	6.56791E-02	6.56791E-02	6.38590E-02
WW	Friedman	1.84926E-10	5.69003E-10	5.69003E-10	5.69003E-10
	Friedman Aligned	3.15599E-13	8.01137E-13	8.01137E-13	8.01137E-13
	Quade	5.31725E-03	1.96611E-02	1.96611E-02	1.94928E-02
DE	Friedman	4.61292E-09	1.59678E-08	1.59678E-08	1.59678E-08
	Friedman Aligned	3.62181E-04	1.33738E-03	1.33738E-03	1.33663E-03
	Quade	7.62673E-02	2.85885E-01	2.49968E-01	2.53918E-01
IJAYA	Friedman	6.88175E-09	2.54096E-08	2.54096E-08	2.54096E-08
	Friedman Aligned	8.79672E-04	3.04543E-03	3.04543E-03	3.04172E-03
	Quade	7.62673E-02	2.85885E-01	2.49968E-01	2.53918E-01
CWOA	Friedman	8.73483E-09	3.29236E-08	3.29236E-08	3.29236E-08
	Friedman Aligned	4.27917E-09	1.58000E-08	1.58000E-08	1.58000E-08
	Quade	2.57827E-03	5.93402E-03	5.93402E-03	5.91840E-03
NNA	Friedman	1.17491E-08	4.33811E-08	4.27586E-08	4.33811E-08
	Friedman Aligned	2.23361E-09	7.25937E-09	7.25937E-09	7.25937E-09
	Quade	2.57827E-03	4.09880E-03	3.90245E-03	4.09117E-03
ISCA	Friedman	1.23525E-08	4.33811E-08	4.27586E-08	4.33811E-08
	Friedman Aligned	<1E-13	<1E-13	<1E-13	<1E-13
	Quade	2.57827E-03	3.65691E-03	3.65691E-03	3.65079E-03
NDE	Friedman	2.55436E-06	7.85957E-06	7.85957E-06	7.85955E-06
	Friedman Aligned	4.19953E-02	1.29854E-01	1.29854E-01	1.23666E-01
	Quade	1.60056E-01	5.02233E-01	5.02233E-01	4.15313E-01
TLBO	Friedman	1.57702E-01	4.05499E-01	4.05499E-01	3.53159E-01
	Friedman Aligned	6.48054E-01	1.0	1.0	9.29409E-01
	Quade	7.18467E-01	1.0	1.0	9.59945E-01
EBLSHADE	Friedman	9.13338E-01	1.0	9.23824E-01	9.89059E-01
	Friedman Aligned	8.67482E-01	1.0	1.0	9.76034E-01
	Quade	9.98363E-01	1.0	1.0	9.99993E-01
STLBO	Friedman	9.23824E-01	1.0	9.23824E-01	9.89059E-01
	Friedman Aligned	1.0	1.0	1.0	1.0
	Quade	1.0	1.0	1.0	1.0

Table 4
Adjusted p-values for Friedman, Friedman Aligned, and Quade tests in IV–set case. STLBO is the control algorithm.

Algorithm	Test	post-hoc procedure			
		Finner	Holm	Hochberg	Holland
GOTLBO	Friedman	<1E-13	<1E-13	<1E-13	<1E-13
	Friedman Aligned	1.35278E-10	5.09895E-10	5.09895E-10	5.09895E-10
	Quade	1.11445E-03	4.11614E-03	4.11614E-03	4.10873E-03
PSO	Friedman	<1E-13	<1E-13	<1E-13	<1E-13
	Friedman Aligned	<1E-13	<1E-13	<1E-13	<1E-13
	Quade	8.22938E-06	8.22941E-06	8.22941E-06	8.22938E-06
NNA	Friedman	<1E-13	<1E-13	<1E-13	<1E-13
	Friedman Aligned	<1E-13	<1E-13	<1E-13	<1E-13
	Quade	2.21284E-05	5.61727E-05	5.61727E-05	5.61713E-05
CWOA	Friedman	<1E-13	<1E-13	<1E-13	<1E-13
	Friedman Aligned	<1E-13	<1E-13	<1E-13	<1E-13
	Quade	1.48311E-05	2.73807E-05	2.73807E-05	2.73803E-05
DE	Friedman	2.32081E-13	8.03357E-13	8.03357E-13	8.03357E-13
	Friedman Aligned	1.74950E-09	6.45968E-09	6.45968E-09	6.45968E-09
	Quade	6.44257E-03	2.38175E-02	2.38175E-02	2.35824E-02
IJAYA	Friedman	2.17645E-10	8.03613E-10	8.03613E-10	8.03613E-10
	Friedman Aligned	3.63299E-09	1.25757E-08	1.25757E-08	1.25757E-08
	Quade	3.78757E-02	1.31885E-01	1.31885E-01	1.25109E-01
MABC	Friedman	1.75608E-09	6.61909E-09	6.61909E-09	6.61909E-09
	Friedman Aligned	<1E-13	<1E-13	<1E-13	<1E-13
	Quade	1.54776E-03	5.83595E-03	5.83595E-03	5.82137E-03
WW	Friedman	7.44635E-09	2.74942E-08	2.74942E-08	2.74942E-08
	Friedman Aligned	<1E-13	<1E-13	<1E-13	<1E-13
	Quade	1.10078E-04	3.81053E-04	3.81053E-04	3.80989E-04
ISCA	Friedman	1.32325E-08	4.58048E-08	4.58048E-08	4.58048E-08
	Friedman Aligned	<1E-13	<1E-13	<1E-13	<1E-13
	Quade	5.64886E-05	1.73815E-04	1.73815E-04	1.73801E-04
NDE	Friedman	9.57698E-04	2.94709E-03	2.94709E-03	2.94383E-03
	Friedman Aligned	2.69373E-03	8.29097E-03	8.29097E-03	8.26522E-03
	Quade	2.98714E-01	9.55486E-01	9.55486E-01	6.64392E-01
EBLSHADE	Friedman	8.62842E-02	2.20533E-01	2.20533E-01	2.04719E-01
	Friedman Aligned	3.10807E-02	7.90881E-02	7.90881E-02	7.70214E-02
	Quade	5.99120E-01	1.0	1.0	9.01765E-01
ADELI	Friedman	1.0	1.0	1.0	1.0
	Friedman Aligned	3.64522E-01	6.83937E-01	3.45600E-01	5.66995E-01
	Quade	1.0	1.0	1.0	1.0
TLBO	Friedman	1.0	1.0	1.0	1.0
	Friedman Aligned	3.64522E-01	6.83937E-01	3.45600E-01	5.66995E-01
	Quade	1.0	1.0	1.0	1.0

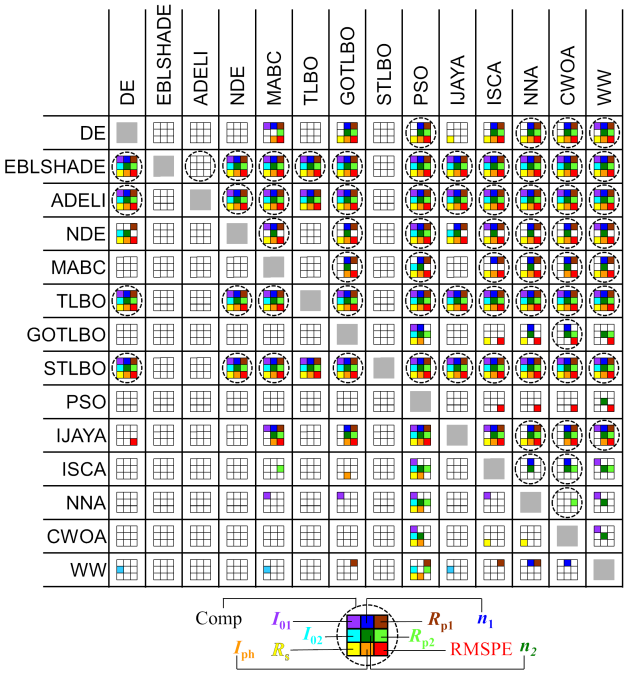

Figure 5: The results of Wilcoxon signed-rank test with a level of significance $\alpha = 0.05$ in the single-IV case. Each colored small square indicates that the algorithm specified in the row outperforms the algorithm specified in the column in evaluating one of the parameters of the two–diode model. The correspondence between the color and position of the square to a model parameter is shown in a legend at the figure bottom. The advantage of the row algorithm in the Comp parameter is indicated by the presence of a dashed circle.

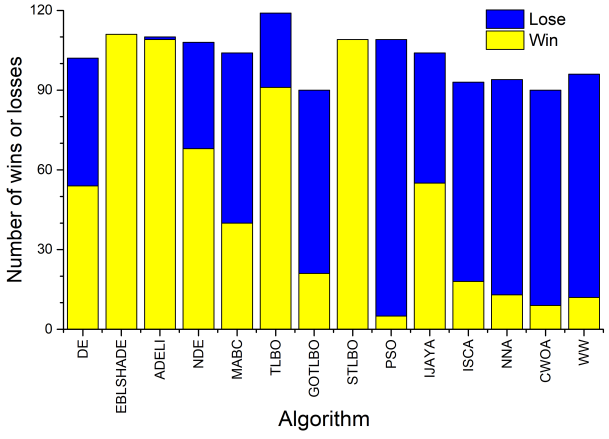

Figure 6: The total number of wins and losses for each algorithm in pairwise comparisons using the Wilcoxon signed-rank test with a significance level of $\alpha = 0.05$ in the single-IV case.

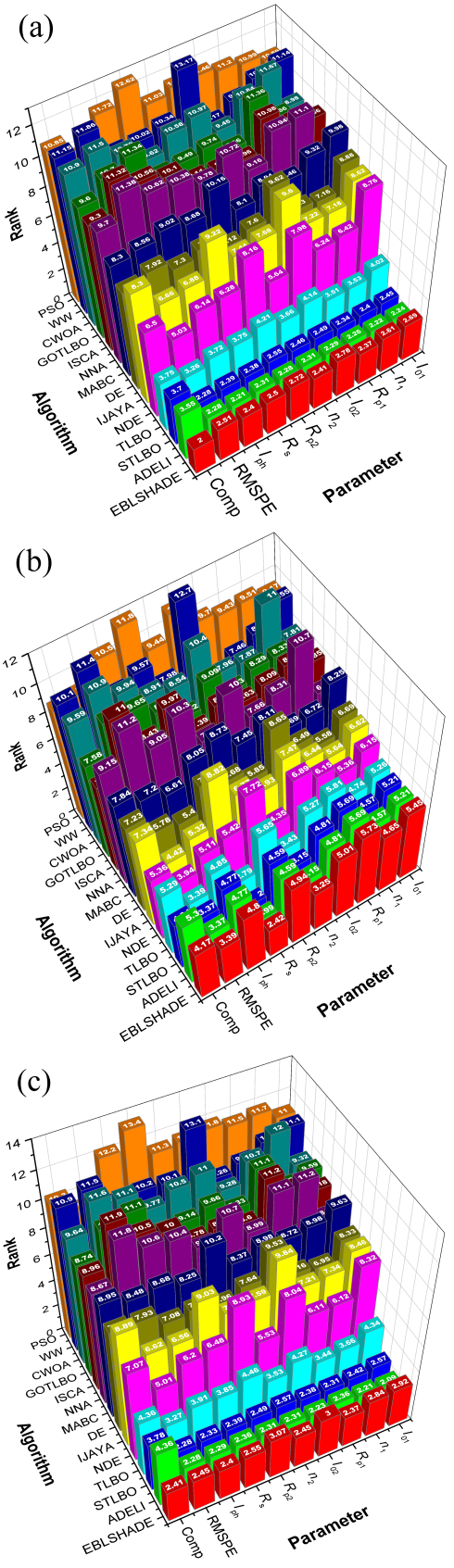

Figure 7: Ranking of the algorithms according to Friedman (a), Friedman Aligned (b), and Quade (c) tests in the single-IV case.

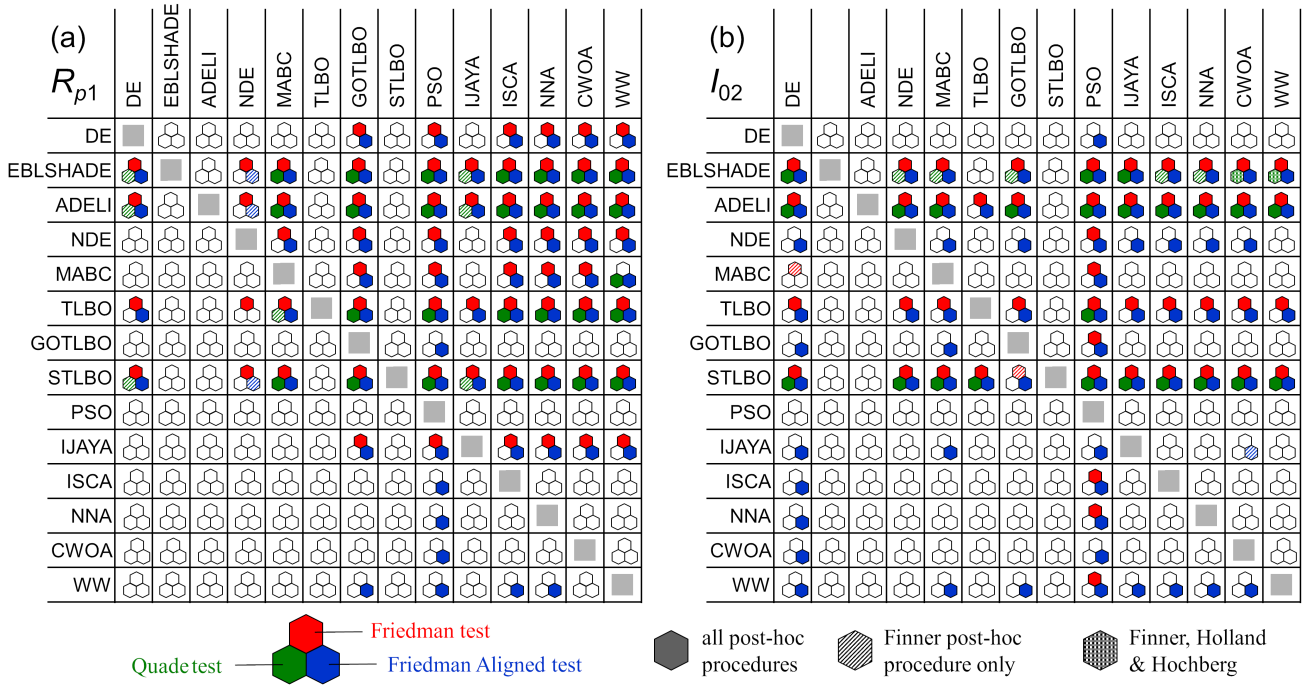

Figure 8: The results of algorithm comparison in R_{p1} (a) and I_{02} (b) evaluation by Friedman, Friedman Aligned, and Quade tests in the single–IV case. The colored hexagon indicates that the adjusted p-value, which tests the hypothesis that an algorithm in a row outperforms the algorithm in a column, is not greater than $p_{lim} = 0.1$. The solid fill signifies that every post-hoc procedure resulted in $p < p_{lim}$; the patterned fill indicates that only specific post-hoc procedures achieved this outcome. The correspondence between the color and position of the hexagon to a test as well as the fill pattern to procedures are shown in a legend at the bottom of the figure.

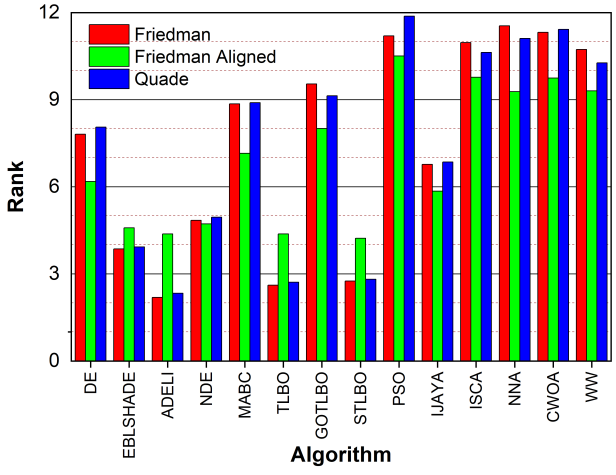

Figure 9: Ranking of the algorithms according to Friedman, Friedman Aligned, and Quade tests in the IV-set case.

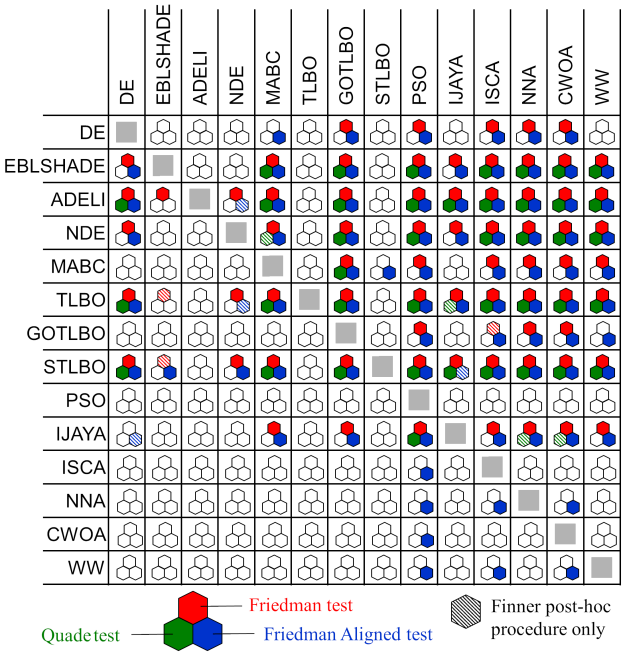

Figure 10: The results of algorithm comparison by Friedman, Friedman Aligned, and Quade tests in the IV-set case. The colored hexagon indicates that the adjusted p-value, which tests the hypothesis that an algorithm in a row outperforms the algorithm in a column, is not greater than $p_{lim} = 0.1$. The solid fill signifies that every post-hoc procedure resulted in $p < p_{lim}$; the dashed fill indicates that the Finner post-hoc procedure was the only method that produced this result. The correspondence between the color and position of the hexagon to a test is shown in a legend at the bottom of the figure.

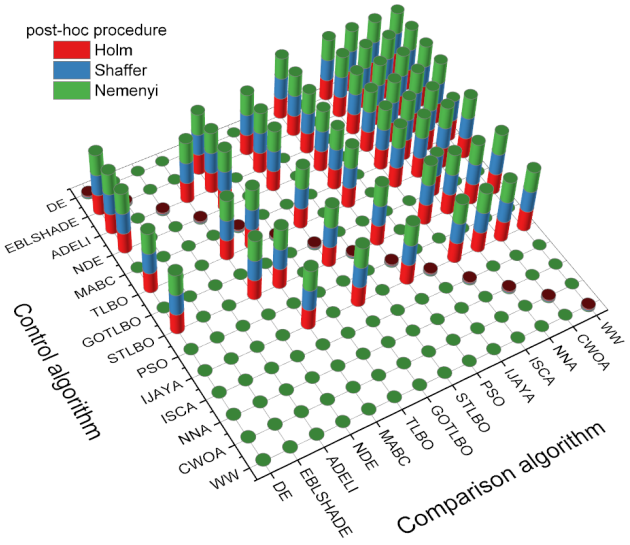

Figure 11: The results of multiple comparisons among all algorithms in the IV-set case. The colored cylinder indicates that the adjusted p-value, which tests the control algorithm outperforms the comparison algorithm, is not greater than $p_{lim} = 0.1$. The correspondence between the color of the hexagon to a post-hoc procedure is shown in a figure legend.